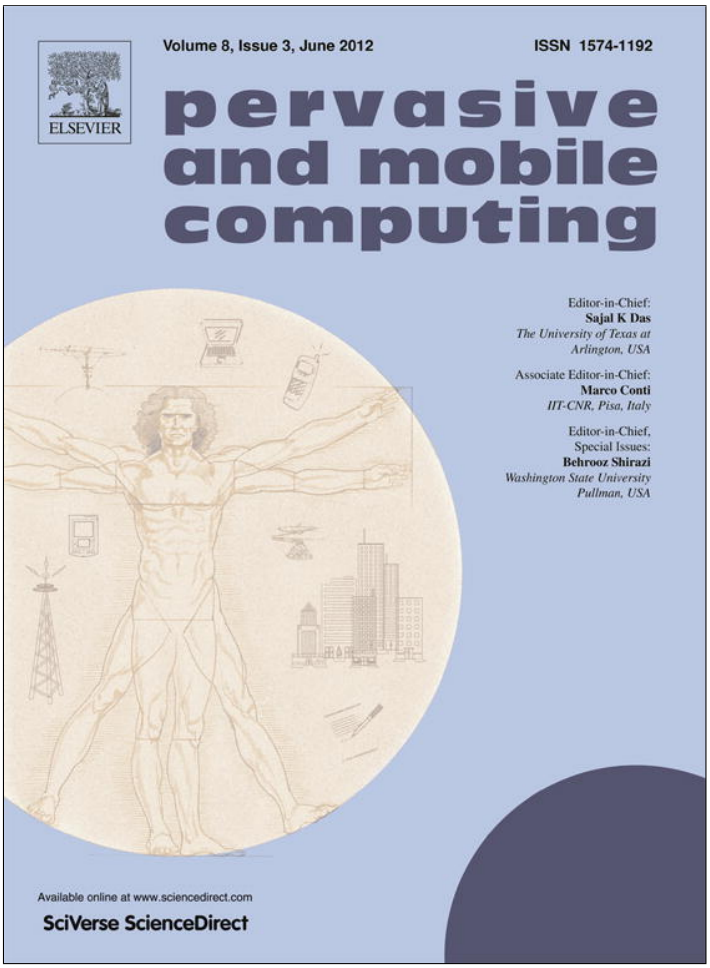

Pervasive and Mobile Computing 8 (2012) 429–447

Contents lists available at SciVerse ScienceDirect

Pervasive and Mobile Computing

journal homepage: www.elsevier.com/locate/pmc

Energy-efficient mobile target detection in Wireless Sensor Networks with random node deployment and partial coverage

Paolo Medagliani [a,*], Jérémie Leguay [c], Gianluigi Ferrari [b], Vincent Gay [c], Mario Lopez-Ramos [c]

[a] Lepida spa, Viale Aldo Moro 64, I-40127 Bologna, Italy

[b] University of Parma, Department of Information Engin., Wireless Ad-hoc and Sensor Networks (WASN) Lab, Viale G. P. Usberti 181/A, I-43124 Parma, Italy

[c] Thales Communications, 160 Bd de Valmy, Colombes Cedex, France

ARTICLE INFO

Article history:
Received 9 April 2010
Received in revised form 16 September 2010
Accepted 15 February 2011
Available online 11 March 2011

Keywords:
Wireless Sensor Network (WSN)
Target detection
Partial coverage
Random node deployment
Probability of missed detection
Latency before detection
Optimization toolbox

ABSTRACT

This paper addresses the problem of engineering energy-efficient target detection applications, using unattended Wireless Sensor Networks (WSNs) with random node deployment and partial coverage, for long-lasting surveillance of areas of interest. As battery energy depletion is a crucial issue, an effective approach consists in switching on and off, according to proper duty cycles, sensing and communication modules of wireless sensor nodes. Making these modules work in an intermittent fashion has an impact on (i) the latency of notification transmission (depending on the communication duty cycle), (ii) the probability of missed target detection (depending on the number of deployed nodes, the sensing duty cycle, and the number of incoming targets), and (iii) the delay in detecting an incoming target. In order to optimize the system parameters to reach given performance objectives, we first derive an analytical framework which allows us to evaluate the probability of missed target detection (in the presence of either single or multiple incoming targets), the notification transmission latency, the detection delay, and the network lifetime. Then, we show how this "toolbox" can be used to optimally configure system parameters under realistic performance constraints.

1. Introduction

Wireless Sensor Networks (WSNs) are formed by battery-powered devices commonly used for environmental monitoring, military surveillance, and industrial automation. Recent advances in hardware miniaturization, low-power radio communications, and battery lifetime, together with the increasing affordability of such devices, are paving the way for a widespread use of WSNs in a vast array of applications. For example, in a natural reserve, a large number of affordable sensor nodes with vibration and acoustic sensors can be spread throughout the monitored area to study environmental conditions and animal behaviors in an unintrusive manner (i.e., without attaching devices to animals). WSNs can also help to attract animals through sounds, to enable interactive applications, such as guiding visitors to animal herds, as well as to protect endangered species from hunters. In these contexts, the whole application functionalities rely on the ability to detect any incoming target (e.g., animal, hunter, etc.) in a given area of interest.

This paper addresses the problem of target detection using a long-term random deployment of sensor nodes over a monitored area. Partial area coverage is considered, i.e., the spatial density of the sensor nodes is typically small, as this could be the case in many realistic surveillance scenarios of large areas. In such vast and long-term deployments, one of

* Corresponding author. Tel.: +39 0521 905759; fax: +39 0521 905758.
E-mail addresses: paolo.medagliani@lepida.it, paolomeda@gmail.com (P. Medagliani), jeremie.LEGUAY@fr.thalesgroup.com (J. Leguay), gianluigi.ferrari@unipr.it (G. Ferrari), vincent.GAY@fr.thalesgroup.com (V. Gay), mario.LOPEZRAMOS@fr.thalesgroup.com (M. Lopez-Ramos).

1574-1192/$ – see front matter © 2011 Elsevier B.V. All rights reserved.
doi:10.1016/j.pmcj.2011.02.004

the main design goals is to maximize the operational lifetime of the system, by cyclically switching on and off the sensing and communication parts, while ensuring that targets will eventually be detected and that the corresponding notification will be transmitted within a given time interval. Although the problem of target detection has been extensively studied in recent years (see, e.g., [1–4]), a complete performance modeling framework is still missing in the context of realistic target detection applications for energy-efficient WSN. In this paper, we further extend the preliminary results presented in [5], deriving a performance analysis framework based on a larger set of relevant metrics. This paper brings the following main contributions: it proposes an analytical framework to characterize the performance of a duty-cycled (at sensing and communication layers) WSN in terms of probability of missed target detection, delay of detection, latency of notification transmission, and average energy consumption. In addition, we present an engineering toolbox which allows to efficiently set the configuration parameters in order to make a WSN function at a desired operating point, characterized by a trade-off between energy consumption and quality of service (in terms of detection capability and latency). We then validate the use of our toolbox to optimally configure a WSN under realistic constraints.

This paper is structured as follows. In Section 2, we discuss relevant related works. In Section 3, we describe the problem and the simulation set-up. In Section 4, we first derive an analytical framework for the evaluation of the probability of missed detection, and we present its assessment using simulation results. Section 5 characterizes the delay required for target detection. Sections 6 and 7 provide analytical models for the evaluation of the latency and of the energy consumption, respectively. In Section 8, we demonstrate how the proposed analytical toolbox can be used to configure a WSN. Finally, Section 9 provides concluding remarks and a list of further works.

2. Related work

In this section, we discuss relevant literature related to the problem of target detection, considering various aspects, such as sensing coverage strategies, modeling efforts, collaborative detection schemes, as well as experimental activities.

Characterizing the detection capability of a WSN has been a topic of extensive research in recent years. In [6], the authors map the target detection problem with a line-set intersection problem and derive an analytic framework for the computation of the target detection probability, under random and deterministic node deployment strategies. In [7,8], the authors use integral geometry tools to tackle the design of target detection systems. In [1], the authors evaluate the benefit brought by the use of mobile sensor nodes for target detection.

The authors of [9,10] review the state-of-the-art cross-layer design techniques for WSNs and propose a taxonomy that encompasses power efficiency-oriented approaches. The duty-cycling techniques considered in our paper fall into this class of approaches. In [2,11,12], the authors present ANDES, an analysis-based design tool to estimate quantitatively various performance metrics of target detection WSNs. While ANDES derives models for the average detection delay and the probability of detection for duty-cycled WSNs, it includes neither an energy-based joint optimization, nor a modeling for off-the-shelf communication protocols. In [13], the authors propose a distributed scheduling algorithm of sensor wake-ups, which reduces the detection delay and the probability of missed detection, under the assumptions that there are (i) global time synchronization and (ii) minimal knowledge, among the sensors, of their relative distances.

Recently, target detection applications with decision reporting to a sink have also received a significant attention. In [14], the authors focus on unattended acoustic sensor network and present a self-organization algorithm for energy-efficient target localization and tracking. In [15], the authors introduce a duty-cycling strategy using magnetic sensors for power-efficient and reliable target detection. The experimental set-ups considered in [14,15] constitute practical implementation examples of the sensing modules which will be considered in the following. In [16], the authors present a framework for sensor deployment, data routing, distributed computing, and information fusion, considering integrated WSNs and wired computer networks. Following an implementation-oriented approach, in [17] the authors present the design and the implementation of a monitoring system, referred to as VigilNet, based on a WSN with the Crossbow MicaZ platform [18]. Their goal is to assess the trade-offs between node spatial density and duration of duty cycle. The analytical framework which will be derived in the following is an analytical counterpart of the experimental VigilNet approach. In [3], under the assumptions that a road network map is known and the target movement is confined into roads, the authors describe an algorithm, referred to as VIrtual Scanning Algorithm (VISA), which guarantees that the incoming target will be detected before reaching a given protection point.

Strategies and techniques for node placement are considered in [19], where the authors propose a taxonomy of possible node deployment strategies (e.g., random vs. deterministic, static vs. dynamic attribution of sink role) and review the existing literature on this subject. They evaluate how random /deterministic node placement strategies to guarantee a minimum network coverage. In [4], the authors propose a density control algorithm for duty-cycled WSNs, studying the relationship between coverage and connectivity. In [20], the benefits of dynamic coverage algorithms, based on sensors with variable transmission and sensing ranges, are evaluated. However, these approaches do not provide a performance characterization in terms of probability of missed target detection in the presence of sensing duty-cycling. In [21], optimized deterministic node placement, with respect to area coverage or network connectivity, is considered, by taking into account a dynamic allocation of the role of sink among the sensor nodes. Our paper presents performance estimators for both detection and networking parts. Albeit derived for a random node placement, these indicators can support a decision process for node deployment. In fact, in [22] we propose a preliminary extension of our framework in the presence of deterministic node deployment.

Collaborative target detection is another topic recently investigated. In [23], the authors propose a data-fusion based collaborative detection scheme for achieving guaranteed accuracy in sensor deployment. In [24], mobile sensors are allowed to collaborate with static sensors, and move reactively to meet desired detection performance requirements. In the framework proposed in the following, the sensor nodes are not mobile and they do not collaborate to make decisions on coverage parameters. However, no costly synchronization among the sensor nodes is required. In our case, the gateway is computing the optimal set of system parameters by looking at the WSN, through analytical models, as a whole. Our models can be extended to consider different sets of parameters for the nodes (duty cycles, sensing range), but this would to lead to a higher complexity of the analytic framework. This is the subject of future research activity.

To summarize, with respect to existing literature in the field of WSN-based target detection, our work is innovative in the following aspects: (i) we derive a "rich" analytical framework which allows to evaluate the impact of power-saving techniques, at both sensing and communication layers, in the case of random node deployment with partial coverage; (ii) the system performance in the presence of multiple targets can be analyzed; (iii) the validity of the predicted performance holds even if target paths are not confined within specific (limited) regions (e.g., roads); and (iv) we propose an engineering toolkit for the energy-efficient WSN configuration.

3. Preliminaries

3.1. The target detection problem

The surveillance of a given area is important in many military and civilian applications. In particular, a WSN can help to detect an incoming target which crosses the monitored area. Upon the detection of a target, an alert message is sent to a gateway node, namely the sink or Access Point (AP), which can reach control centers outside the network. The operational point of a WSN can be characterized using a number of performance metrics of interest, including the probability of missing a single incoming target (denoted P_{md}) and, in the context of multiple targets entering simultaneously the area, the probabilities of missing all incoming targets (denoted as P_{ma}) or at least one of the incoming targets (denoted as P_{mo}). In the following, we also consider the delay for detecting a target (denoted as D_{det}), the notification transmission latency (denoted as D), and the network lifetime (denoted as $\mathcal{L}$).

The problem of target detection using a long-term deployment of a WSN lies in the unavoidable trade-offs that energy-saving strategies raise in terms of detection capability, responsiveness, and network lifetime. In these battery-powered networks, nodes are cyclically "switched off", according to proper duty cycles at both sensing and communication levels, in order to save energy. However, while extending the network lifetime, these operations have also impacts on: (i) P_{md}, P_{ma}, P_{mo}, and D_{det}, since a node may be off when the target crosses its sensed area; (ii) D, since sleeping nodes can delay the transmission of an alert message towards the AP.

This paper aims at providing an analytical framework for the aforementioned performance metrics, taking into account the impact of duty-cycling techniques. After validating the derived analytical models, the last part of the paper provides a practical application case, which shows how an operator (i) can predict the performance of a deployed WSN in realistic scenarios and (ii) can assess the trade-offs that arise when favoring one performance metric over another.

3.2. WSN model

The main parameters of the overall system model are listed in Table 1. The device-specific values presented in this table have been taken from the internal data-sheet of a prototype sensor node by Thales. Like other well-known commercial sensor nodes using the CC2420 chipcon (e.g., [25,26]), power consumption is higher in the reception mode than in the full-power transmission mode.

The wireless sensor devices considered in this paper embed two main sub-units: (i) the sensing sub-unit and (ii) the communication sub-unit. The former is equipped with a seismic sensor, whose sensing range r_{s} (dimension: [m]) is largest over a rocky surface, in which the vibrations due to an incoming target propagate with low attenuation. Since seismic sensors can be placed over different surfaces, such as sandy or clayey terrains, where the propagation model is different and the attenuation is higher, we consider different values of r_{s}. In order to reduce the energy consumption of the system, the sensing part can be periodically switched off, according to a normalized duty cycle, over a period of duration t_{sens} (dimension: [s]), identified by the parameter $\beta_{\mathrm{sens}} \in (0, 1]$. More precisely, over each period nodes sense the surrounding environment for an interval of length $\beta_{\mathrm{sens}} t_{\mathrm{sens}}$ and sleep for an interval of duration $(1 - \beta_{\mathrm{sens}}) t_{\mathrm{sens}}$; then, the duty cycle starts over in the consecutive period. The power consumption associated with the sensing operations is denoted as Ω_{sens} (dimension: [W]). We assume that all sensor nodes have the same values of r_{s}, β_{sens}, and t_{sens}.

The communication sub-unit is characterized by a transmission range r_{T} (dimension: [m]), with $r_{\mathrm{T}} \gg r_{\mathrm{s}}$. Generally, r_{T} ranges between 100 m and 1000 m (in line-of-sight scenarios). In the remainder of the paper, r_{T} will be set to 250 m. As for the sensing sub-unit, duty-cycling is also considered for the communication sub-unit. In this case, the period of the duty cycle is denoted as t_{comm} (dimension: [s]) and the percentage of this period during which the communication sub-unit is on is given by the parameter $\beta_{\mathrm{comm}} \in (0, 1]$.

In the following, we assume that only the first node detecting the target transmits an alert message to the AP. In the derivation of latency after target detection model (Section 6), we balance the assumption of collision-free transmission

Table 1
Constant and variable system parameters considered in the simulations.

Constant parameters			
Side of monitored area	d_s	1000 m	Scenario-specific
Speed of the target	v	15 m/s	Scenario-specific
Sensing power consumption	Ω_{sens}	0.0036 W	Device-specific
Average number of hops	N_{hop}	3	Function of the number of nodes in the network
Transmission range	r_T	250 m	Device-specific
Preamble duration	S_p	0.26 ms	Configuration-specific
Ack window duration	S_{al}	0.26 ms	Configuration-specific
Packet duration	S_d	0.93 ms	Application-specific
Transmission power consumption	Ω_{Tx}	0.0511 W	Device-specific
Reception power consumption	Ω_{Rx}	0.0588 W	Device-specific
Sleep power consumption	Ω_s	$2.4 \cdot 10^{-7}$ W	Device-specific
Variable parameters (with default value ranges)			
Number of nodes in the network	N	[10 ; 70] (50)	Scenario-specific
Sensing range of each node	r_s	20, 35, 50 (50) m	Device-specific
Sensing duty cycle	β_{sens}	[0.1 ; 1]	Configuration-specific
Sensing period	t_{sens}	[5 ; 25] (15) s	Configuration-specific
Communication duty cycle	β_{comm}	[0.0025 ; 1]	Configuration-specific
Communication period	t_{comm}	40, 80, 100, 120 (100) ms	Configuration-specific
Number of incoming targets	N_T	1, 2, 4, 8	Scenario-specific

with respect to the node spatial density and the number of incoming targets. In a surveillance scenario, the Medium Access Control (MAC) protocol must guarantee the lowest energy consumption and the lowest latency. In the following, we consider a specific MAC protocol for the derivation of the analytical framework. More precisely, we choose the X-MAC protocol [27] which is suitable for low throughput and low latency communications. This random access protocol notably outperforms most scheduled MAC protocols, as shown in [28]. In Section 6, we provide more details on the X-MAC protocol and its corresponding main parameters (namely, S_d, S_p, S_{al}, Ω_{Tx}, Ω_{Rx}, and Ω_s), whose reference values are indicated in Table 1. The derived models for latency (Section 6) and network lifetime (Section 7) are specific to the X-MAC protocol. They allow us to give some examples of system engineering with a practical application case in Section 8. We remark, however, that the proposed framework can be extended to other MAC protocols by properly modeling the corresponding communication layers.

We assume the monitored area to be a square with sides of length d_s (dimension: [m]), over which N sensors are independently randomly deployed. In Section 4, we derive an analytical lower bound on the probability of missed detection, under the constraint of non-overlapped sensed areas. The validity and tightness of this bound, with respect to the performance in the case of random node deployment (with possibly overlapped areas) is investigated. We also assume that the potential targets cross the monitored area following straight line trajectories, as shown in Fig. 1. Each trajectory is uniquely identified by (i) an entrance point over the perimeter of the monitored area, uniformly distributed in $[0, 4d_s]$; (ii) an entrance angle, with respect to a reference axis given by the entrance side, uniformly distributed in $[0, \pi]$; and (iii) a constant target speed v (dimension: [m/s]).

4. Probability of missed target detection

4.1. Preliminary background: non-overlapped sensed areas

Our analytical framework for the evaluation of the probability of missed target detection extends the results presented in [6], which we briefly review in the following. For more details about the proposed derivation, the interested reader is referred, besides to [6], also to [7,8].

In order to detect a target in a square area with perimeter l_0, assume that N sensors, denoted as $\{s_i\}_{i=1}^N$ are randomly placed over this area. The perimeter of the area sensed by the ith sensor s_i is denoted as l_i. Assuming that there is no prior knowledge about the direction and the entrance point of the target and that sensed areas of different sensors do not overlap, the probability $P_d(k)$ that at least $k \geq 1$ sensors detect the target crossing the field of interest can be expressed as [6]

$$P_d(k) = 1 - \sum_{w=0}^{k-1} \binom{N}{w} \sum_{j=1} \prod_{i=1}^{w} q_{z_j^{(w)}(i)} \prod_{v=1}^{N-w} (1 - q_{\bar{z}_j^{(w)}(v)}) \tag{1}$$

where: $\binom{N}{w}$ is the number of possible combinations of N objects in groups of w; $\mathbf{z}_j^{(w)}$ denotes the jth w-tuple $\{z_j^{(w)}(1), z_j^{(w)}(2), \ldots, z_j^{(w)}(N)\}$ extracted from the set of integers $\{1, 2 \ldots, N\}$ (i.e., $z_j^{(w)}(i) \in \{1, 2 \ldots, N\}, \forall i$) and $z_j^{(w)}(i) \neq z_j^{(w)}(h)$;

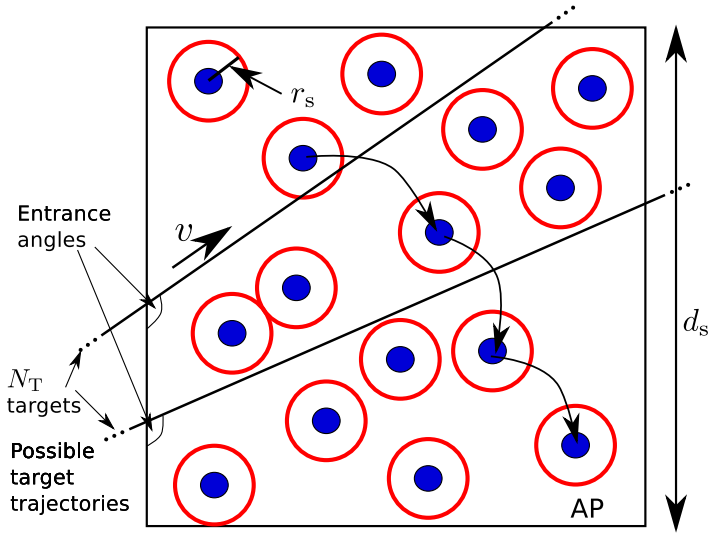

Fig. 1. Illustrative example of WSN scenario for target detection.

$\bar{\mathbf{z}}_j^{(w)}$ denotes the jth $(N-w)$-tuple complement of $\mathbf{z}_j^{(w)}$ (i.e., $\bar{\mathbf{z}}_j^{(w)} = \{1,2,\ldots,N\} \setminus \mathbf{z}_j^{(w)}$); and $q_h \triangleq P\{\text{Sensor } h \text{ is on the trajectory}\}$. Since $q_h = l_h/l_0$, (1) becomes:

$$P_d(k) = 1 - \sum_{w=0}^{k-1} \sum_{j=1}^{\binom{N}{w}} \underbrace{\prod_{i=1}^{w} \frac{l_{z_j^{(w)}(i)}}{l_0} \prod_{v=1}^{N-w} \left(1 - \frac{l_{\bar{z}_j^{(w)}(v)}}{l_0}\right)}_{(*)}. \tag{2}$$

In other words, the term $(*)$ represents the probability that w sensors (identified by the jth possible configuration) detect the target and the other $N-w$ do not.

For the sake of analytical simplification, assuming that the perimeters of the sensed areas are all equal, i.e., $l_h = l \ \forall h \in \{1,\ldots,N\}$, the probability of missed detection in (2) reduces to

$$P_d(k) = 1 - \sum_{w=0}^{k-1} \binom{N}{w} \frac{l^w (l_0 - l)^{N-w}}{l_0^N}.$$

Since $P_{md} = 1 - P_d(1)$, from (2) it follows:

$$P_{md} = \sum_{w=0}^{0} \sum_{j=1}^{1} \underbrace{\prod_{i=1}^{w} \frac{l_{z_j^{(0)}(i)}}{l_0}}_{=1} \prod_{v=1}^{N} \left(1 - \frac{l_{\bar{z}_j^{(0)}(v)}}{l_0}\right) = \prod_{v=1}^{N} \left(1 - \frac{l_v}{l_0}\right) \tag{3}$$

where we have used the fact that $\bar{\mathbf{z}}_j^{(0)} = \{1,2,\ldots,N\}$. Intuitively, referring to the term at the right-hand side of (3), P_{md} depends only on the length of the perimeters $\{l_v\}_{v=1}^N$ of the sensed areas and the perimeter l_0 of the monitored area, regardless of the length of the target trajectory inside the monitored area and of the positions of the sensors. We point out that, since $P_d(1)$ is the probability that a target is detected by at least one sensor (and *not* by exactly one sensor), the computation of P_{md} does not depend on the fact that a target may have already been detected by other sensors. Instead, we simply evaluate the probability that a generic sensor detects the incoming target, neglecting what the other sensors have done.

According to the model introduced in Section 3.2 and recalling that all the sensors have the same sensing range, Eq. (3) can be rewritten as follows:

$$P_{md} = \left(1 - \frac{2\pi r_s}{4 d_s}\right)^N \tag{4}$$

where $2\pi r_s/(4d_s)$ is the probability that a target is on the trajectory [6]. Note that the constraint of non-overlapped circular sensed areas automatically implies partial coverage with detection holes.

We remark that Eq. (4) holds in scenarios where the sensed areas of the nodes are not overlapped. In the presence of overlapping, Eq. (4) should be refined to take into account that the overall perimeter of the overlapped sensed areas is shorter than the sum of all perimeters of the single sensed areas. Therefore, in the presence of overlapping the coverage guaranteed by the sensor nodes reduces and so does the network ability to detect a target. In other words, the approach

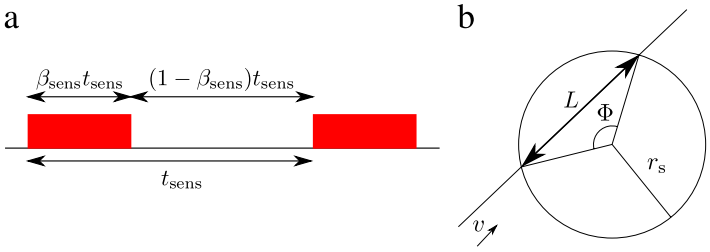

Fig. 2. (a) Logical scheme of the sensing duty cycle and (b) model for the sensing range of a node.

proposed in [6] allows to derive a lower bound on the probability of missed detection in the presence of random node deployment. The evaluation of the exact probability of missed detection in the latter scenario is analytically difficult and deployment-dependent. In order to carry it out, we will resort to simulations.

4.2. Integration of sensing duty cycles

To integrate sleeping duty cycles at the sensing level, we extend the model outlined in Section 4.1 to derive a lower bound on the probability of missed detection as a function of both the sensing duty cycle β_{sens} and the topology of the WSN.

The probability that a single sensor detects a target corresponds to the probability that the following two events are simultaneously verified: (i) the target's trajectory crosses the area sensed by the sensor (event denoted as $\mathcal{E}_{\text{SoT}}$) *and* the sensor detects a target crossing its sensed area[1] (event denoted as $\mathcal{E}_{\text{det}}$). We point out that the area sensed by a node is fully covered, i.e., if a target crosses the sensed area of a sensor when the latter is on, it is detected with probability equal to 1. Therefore, the probability that a specific sensor detects a target, denoted as $P_{\text{d-ss}}$, can be expressed as

$$P_{\text{d-ss}} = P\{\mathcal{E}_{\text{SoT}}, \mathcal{E}_{\text{det}}\} = P\{\mathcal{E}_{\text{det}}|\mathcal{E}_{\text{SoT}}\}P\{\mathcal{E}_{\text{SoT}}\}.$$

As observed after (4), $P\{\mathcal{E}_{\text{SoT}}\}$ can be expressed as $2\pi r_{\text{s}}/(4d_{\text{s}})$. In order to evaluate $P\{\mathcal{E}_{\text{det}}|\mathcal{E}_{\text{SoT}}\}$, we consider the scheme for the sleeping duty cycle presented in Fig. 2(a). Since the target arrives with a finite speed v, the crossing time of the sensed area is $T_{\text{cross}} = L/v$, where L is a random variable which represents the length of the intersection between the target trajectory and the area sensed by a sensor, as shown in Fig. 2(b). Since there is no information about the target arrival instant, this is assumed uniformly distributed over the period duration t_{sens}. When the sensor is on (i.e., during the subinterval of duration $\beta_{\text{sens}}t_{\text{sens}}$), any incoming target will be detected. In the case that the sensor is off, i.e., during the subinterval of duration $(1-\beta_{\text{sens}})t_{\text{sens}}$, the analysis has to be refined. Let $\mathcal{E}_{\text{target}}$ be the event[2] {The sensor is on at the instant at which the target enters the sensed area}. Applying the total probability theorem [29], $P\{\mathcal{E}_{\text{det}}|\mathcal{E}_{\text{SoT}}\}$ can then be expressed as

$$P\{\mathcal{E}_{\text{det}}|\mathcal{E}_{\text{SoT}}\} = P\{\mathcal{E}_{\text{det}}|\mathcal{E}_{\text{target}}, \mathcal{E}_{\text{SoT}}\}P\{\mathcal{E}_{\text{target}}|\mathcal{E}_{\text{SoT}}\} + P\{\mathcal{E}_{\text{det}}|\bar{\mathcal{E}}_{\text{target}}, \mathcal{E}_{\text{SoT}}\}P\{\bar{\mathcal{E}}_{\text{target}}|\mathcal{E}_{\text{SoT}}\} \tag{5}$$

where $P\{\mathcal{E}_{\text{det}}|\mathcal{E}_{\text{target}}, \mathcal{E}_{\text{SoT}}\} = 1$, as $\mathcal{E}_{\text{target}} \subset \mathcal{E}_{\text{det}}$. Since $\mathcal{E}_{\text{target}}$ and $\mathcal{E}_{\text{SoT}}$ are independent – in fact, the activity cycle of a sensor does not depend on the target – one can write

$$P\{\mathcal{E}_{\text{target}}|\mathcal{E}_{\text{SoT}}\} = P\{\mathcal{E}_{\text{target}}\} = \int_0^{\beta_{\text{sens}}t_{\text{sens}}} \frac{1}{t_{\text{sens}}}\text{d}t = \beta_{\text{sens}}$$

and, therefore, $P\{\bar{\mathcal{E}}_{\text{target}}|\mathcal{E}_{\text{SoT}}\} = 1-\beta_{\text{sens}}$. We are now going to evaluate the last probability at the right-hand side of (5), i.e., $P\{\mathcal{E}_{\text{det}}|\bar{\mathcal{E}}_{\text{target}}, \mathcal{E}_{\text{SoT}}\}$. According to the conditioning on $\bar{\mathcal{E}}_{\text{target}}$ and $\mathcal{E}_{\text{SoT}}$, the target arrival time, denoted as T_{a}, is a random variable uniformly distributed over an interval of length $(1-\beta_{\text{sens}})t_{\text{sens}}$. To have successful detection, the target must remain in the sensed area until the sensor turns its sensing device on in the following active period. In this case as well, one must distinguish between two cases: (i) $T_{\text{cross}} > (1-\beta_{\text{sens}})t_{\text{sens}}$ and (ii) $T_{\text{cross}} < (1-\beta_{\text{sens}})t_{\text{sens}}$. In the former case, the target will be detected, since it remains in the sensed area for a time interval longer than the sleeping interval, i.e., $P\{\mathcal{E}_{\text{det}}|\bar{\mathcal{E}}_{\text{target}}, \mathcal{E}_{\text{SoT}}\} = 1$. Therefore, in this case $P\{\mathcal{E}_{\text{det}}|\mathcal{E}_{\text{SoT}}\} = 1$ and, thus, $P_{\text{d-ss}} = P\{\mathcal{E}_{\text{SoT}}\}$. In the latter case, instead, the target will be detected if it enters the sensed area in the last part of the sensor sleeping interval, so that it will be detected in its following active period. In this case, the evaluation of $P\{\mathcal{E}_{\text{det}}|\mathcal{E}_{\text{SoT}}\}$ in (5) can be carried out as follows.

Let us preliminary observe that, since T_{a} and T_{cross} are independent, their joint probability density function (pdf) can be expressed as the product of the marginal pdfs, i.e., $f_{T_{\text{a}},T_{\text{cross}}}(t,\tau) = f_{T_{\text{a}}}(t)f_{T_{\text{cross}}}(\tau)$. We have already noted that

[1] Assuming "instantaneous" detection once the sensing sub-unit is on, the event that a sensor detects a target crossing its sensed area corresponds to the event that the sensor is on for at least an instant while the target is crossing its sensed area.

[2] Note that the event $\mathcal{E}_{\text{det}}$ is verified (i) if the sensor is on at the instant at which the target enters the sensed area (this is event $\mathcal{E}_{\text{target}}$) or (ii) if, given that the sensor is off at the instant at which the target enters the sensed areas, it becomes on before the target exits the sensed area along its trajectory. Therefore, $\mathcal{E}_{\text{target}} \subset \mathcal{E}_{\text{det}}$.

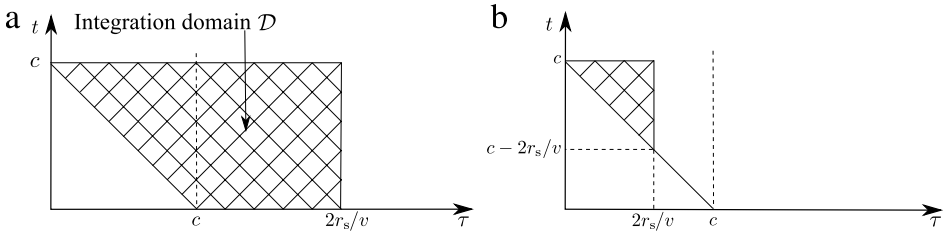

Fig. 3. Integration domain for the evaluation of $P\{\mathcal{E}_1\}$: (a) $2r_s/v > c$ and (b) $2r_s/v < c$.

$T_a \sim \text{Unif}[0, c]$, where $c \triangleq (1 - \beta_{sens})t_{sens}$. In order to express $f_{T_{cross}}(\tau)$, further considerations are required. First of all, $f_{T_{cross}}(\tau) = f_L(\tau)/v$. The length L of the chord can be expressed as follows:

$$L = 2r_s \sin\left(\frac{\Phi}{2}\right)$$

where Φ is the angle shown in Fig. 2(b). Since $\Phi \sim \text{Unif}[0, 2\pi]$, by applying the fundamental theorem [29, p. 93] it can be shown that

$$f_L(\tau) = \begin{cases} \dfrac{1}{\pi\sqrt{r_s^2 - \left(\frac{\tau}{2}\right)^2}} & \text{if } 0 < \tau < 2r_s \\ 0 & \text{otherwise.} \end{cases}$$

Therefore, $f_{T_{cross}}(\tau)$ can be found and one can finally write:

$$f_{T_a,T_{cross}}(t,\tau) = \begin{cases} \dfrac{v}{\pi c\sqrt{r_s^2 - \left(\frac{v\tau}{2}\right)^2}} & \text{if } 0 < \tau < \dfrac{2r_s}{v} \text{ and } 0 < t < c \\ 0 & \text{otherwise.} \end{cases}$$

Letting $\mathcal{E}_1 \triangleq \{T_a + T_{cross} > (1 - \beta_{sens})t_{sens}\}$, given that the sensor is in the sleeping state when the target enters the sensed area, the probability that the target is detected can be expressed as

$$P\{\mathcal{E}_{det}|\bar{\mathcal{E}}_{target}, \mathcal{E}_{SoT}\} = P\{\mathcal{E}_1\} = \iint_{\mathcal{D}} f_{T_a,T_{cross}}(t,\tau)\,dt\,d\tau$$

where the integration domain $\mathcal{D}$ is shown in Fig. 3, where two possible cases are distinguished: (i) $2r_s/v > c$ and (ii) $2r_s/v < c$. In the former case, the integration domain has the trapezoidal shape shown in Fig. 3(a), and $P\{\mathcal{E}_1\}$ can be evaluated as

$$\begin{aligned} P\{\mathcal{E}_1\} &= \int_0^c \int_{c-\tau}^c f_{T_a,T_{cross}}(t,\tau)\,dt\,d\tau + \int_c^{\frac{2r_s}{v}} \int_0^c f_{T_a,T_{cross}}(t,\tau)\,dt\,d\tau \\ &= \frac{4r_s - 2\sqrt{4r_s^2 - c^2v^2}}{\pi cv} + 1 - \frac{2\text{asin}\left(\frac{cv}{2r_s}\right)}{\pi}. \end{aligned} \tag{6}$$

In the latter case, i.e., when $2r_s/v < c$, the integration domain $\mathcal{D}$ reduces to the isosceles triangle, with side $2r_s/v$, shown in Fig. 3(b). $P\{\mathcal{E}_1\}$ can thus be expressed as

$$P\{\mathcal{E}_1\} = \int_0^{\frac{2r_s}{v}} \int_{c-\tau}^c f_{T_a,T_{cross}}(t,\tau)\,dt\,d\tau = \frac{4r_s}{\pi cv}. \tag{7}$$

Combining Eqs. (7) and (6) into Eq. (5), the following expression for $P\{\mathcal{E}_{det}|\mathcal{E}_{SoT}\}$ (in the case with $T_{cross} < (1-\beta_{sens})t_{sens}$) can be obtained:

$$P\{\mathcal{E}_{det}|\mathcal{E}_{SoT}\} = \beta_{sens} + (1 - \beta_{sens})P\{\mathcal{E}_1\}$$

where $P\{\mathcal{E}_1\}$ depends on the relation between $2r_s/v$ and c.

Finally, extending the model in order to take into account that N independent sensors can detect the target, the probability of missed detection with random node deployment can be lower bounded as follows:

$$\begin{aligned} P_{md} &\geq (1 - P_{d-ss})^N = [1 - P\{\mathcal{E}_{det}|\mathcal{E}_{SoT}\}P\{\mathcal{E}_{SoT}\}]^N \\ &= \left\{1 - [\beta_{sens} + (1 - \beta_{sens})P\{\mathcal{E}_1\}]\,\frac{2\pi r_s}{4d_s}\right\}^N \end{aligned} \tag{8}$$

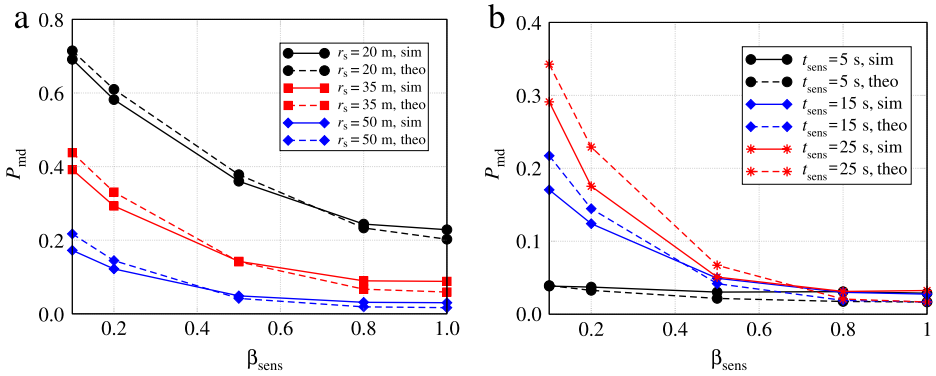

Fig. 4. Simulation (solid lines) and analytical (dashed lines) P_{md} results as functions of the duty cycle β_{sens} considering (a) different values of r_s ($t_{sens} = 15$ s) and (b) different values of t_{sens} ($r_s = 50$ m). In all cases, the target enters with speed $v = 15$ m/s a monitored area of $d_s = 1000$ m side, where $N = 50$ sensors are randomly deployed.

where the expression of $P\{\mathcal{E}_1\}$ depends on the scenario of interest. The expression at the right-hand side of (8) is the exact probability of missed detection with non-overlapped sensed areas. As will be shown in the following subsection by simulation, in the presence of random node deployment (without any constraint on the overlapping) the discrepancy between the lower bound and the exact probability of missed detection becomes more significant for high node spatial density.

In the case of a heterogeneous sensing model (i.e., with different sensing ranges across the sensor nodes), the derivation would be similar, the only difference being that the derivation should start from Eq. (3) rather than from Eq. (4).

4.3. Simulation-based validation

In order to validate the performance results predicted by the analytical framework, we also present simulation results using a custom-based simulator written partly in C and partly in Matlab.[3] To reduce possible statistical fluctuations, each performance value is obtained by simulating at least 1000 different scenarios, corresponding, each of which corresponds to a random nodes' placement, according to a bidimensional uniform distribution, of N nodes over the monitored area. For each scenario, we consider 1000 different target trajectories.

In order to investigate the performance in the absence of overlapping between the sensed areas, after generating a scenario (i.e., after random deployment of the nodes) the corresponding node placement is analyzed: if there is overlapping, the scenario is discarded; otherwise, it is kept.

Another constraint for scenario generation is that every sensor node must communicate with the AP, either directly (one-hop communication) or through intermediate nodes (multi-hop communication). In order to guarantee that a node can always reach the AP upon target detection, after generating a scenario, its connectivity is analyzed: if there are "isolated" nodes (which cannot reach the AP) the scenario is dropped; otherwise, it is kept.

4.3.1. (Pseudo-)Random node deployment with overlapped sensed areas

In Fig. 4(a), P_{md} is shown as a function of β_{sens}, for various values of r_s (t_{sens} is set to 15 s). The number of nodes N is set to 50 and the speed of the target is $v = 15$ m/s. As the intuition might suggest, the longer the sensing range, the higher the probability of detecting an incoming target. When the value of β_{sens} becomes small, the target can cross the sensed area, during a sleeping interval of a sensor, without being detected, thus increasing the probability of missed detection. In Fig. 4(a), simulation results (solid lines) are compared with theoretical ones (dashed lines). As one can see, simulation and analytical results are in good agreement, especially for large values of r_s, confirming the validity of the analytical model.

In Fig. 4(b), P_{md} is evaluated as a function of β_{sens} (r_s is set to 50 m). In all cases, the target speed v is set to 15 m/s. In this case, the same considerations carried out for Fig. 4(a) still hold. When t_{sens} is sufficiently small, β_{sens} has a limited impact on P_{md}. On the other hand, the longer t_{sens}, the stronger the impact of β_{sens}. When $\beta_{sens} = 1$, the sensing period has no impact on the system performance. Instead, when $\beta_{sens} < 1$, a longer t_{sens} leads to a higher P_{md}, because it is more likely a target crosses the sensed area during the sleeping phase of the sensor, without being detected. In this case as well, there is a good agreement between the simulation (solid lines) and theoretical (dashed lines) results. We point out that there is a threshold value of v, depending on r_s, β_{sens}, and t_{sens}, below which the impact of β_{sens} on P_{md} becomes negligible and the curves tend to reach a floor. For instance, with $v = 1.5$ m/s, a target crosses the sensed area for a time interval long enough so that any sensor along its trajectory will detect it, regardless of its duty cycles.

[3] The simulator may be available by contacting the reference author of this paper.

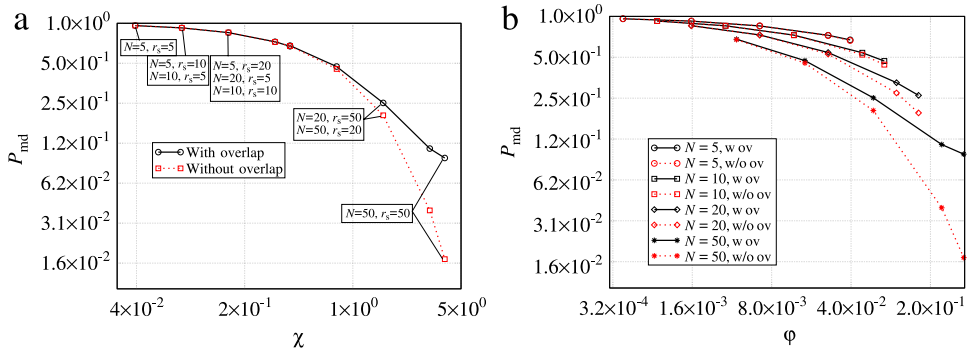

Fig. 5. Probability of missed detection as a function of (a) χ and (b) φ. In both cases, the performance without overlapped sensed areas (w/o ov, simulations) and that with overlapped sensed areas (w ov, analysis) are shown. In both cases, Various values of N and r_s are considered.

4.3.2. Random node deployment

In this subsection, we assess the tightness of the analytical lower bound for the probability of missed detection in the presence of random node deployment. In order to characterize the sparsity of a deployment, we introduce the following two indicators:

$$\chi \triangleq N \cdot \frac{2\pi r_s}{4d_s}$$

$$\varphi \triangleq N \cdot \frac{\pi r_s^2}{d_s^2}$$

where χ is the ratio between (i) the sum of the perimeters of the sensed areas and (ii) the perimeter of the monitored area, whereas φ is the ratio between the (i) sum of the areas sensed by the sensor nodes and (ii) the total monitored area. We now evaluate the probability of missed detection as a function of these two new indicators: without overlapped sensed areas (using the analytical framework) and with possibly overlapped sensed areas (by simulations, considering a purely random node distribution, such that sensors might fall close to each other and the corresponding sensed areas might overlap). We preliminary consider the case with the absence of sensing duty-cycling, i.e., with $\beta_{sens} = 1$. The obtained results are shown in Fig. 5, where the probability of missed detection is shown as a function of (a) χ and (b) φ.

On the basis of the obtained results, the following considerations can be carried out.

- Considering Fig. 5(a), the smaller χ, the better the analytical approximation. In fact, a small value of χ is representative of a scenario where the sum of the perimeters is small with respect to the perimeter of the area, i.e., a scenario where a few nodes are deployed and/or the sensing range of each node is small, so that it is likely that the sensed areas do not overlap. On the other hand, when χ is high, sensed areas have better chance to overlap, thus reducing the detection capability of the system. In this case, the "effective" perimeter of the overlapped sensed areas is smaller than the sum of the perimeters of the nodes. Therefore, considering Eq. (4), the probability of missed detection is higher than the one predicted by the analytical framework in the absence of overlapping.
- Considering Fig. 5(a), the probability of missed detection, with both random node deployment (with possible overlapping) and node deployment with no overlapping, depends only on χ. In other words, given χ it is possible to predict the probability of missed detection of the designed system. This has a remarkable impact from a design perspective.
- Considering Fig. 5(b), since φ can be expressed as a function of χ, there is a behavior similar to Fig. 5(a), that is for low values of φ, the performance with random node deployment (simulation results) is very close to that with no overlapping (analytical results). On the opposite, the higher φ, the larger the gap between simulation and analytical results. It is worth observing that the probability of missed detection does not simply depends on φ, but it is necessary to know also another network parameter (e.g., N or r_s).

While the results shown in Fig. 5 are carried out considering $\beta_{sens} = 1$, it is of interest to evaluate the impact of duty-cycling by keeping the values of χ and φ fixed. In Fig. 6, the probability of missed detection is given as a function of β_{sens}, by considering fixed values of either (a) χ or (b) φ. Referring to Fig. 6(a), where different values of χ are considered, when $\beta_{sens} = 1$ the same performance in Fig. 5(a) is (obviously) obtained. It can be observed that for small values of β_{sens}, the performances with and without overlapping tend to become similar. This is due to the fact that when β_{sens} is small, since the duty cycles of different nodes are not synchronized, it is likely that even if sensed areas overlap, they turn on separately. Therefore, the performance predicted by the analytical framework becomes more accurate also for a scenario with random node deployment. We also remark that while the probability of missed detection, in the case with $\beta_{sens} = 1$, depends only on the value of χ, this is no longer true for $\beta_{sens} < 1$. This is expected from (8), which shows that, when the duty cycle is considered, the performance depends not only on the ratio between the perimeters, but also on the target speed and the time required by a target to cross a sensed area. Considering the results in Fig. 6(b), similar considerations to those for

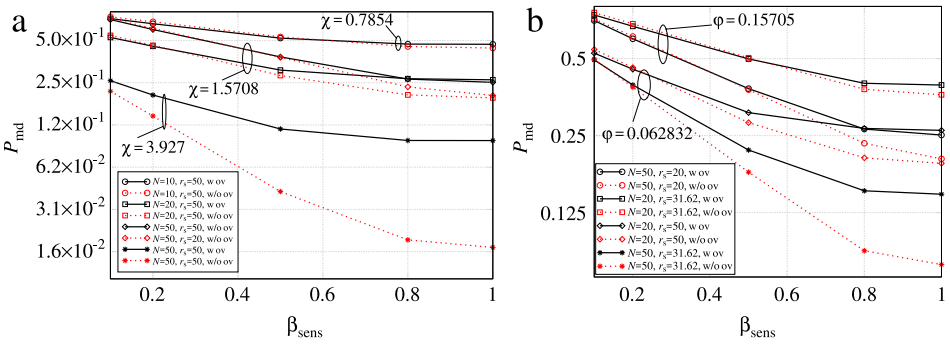

Fig. 6. Probability of missed detection as a function of β_{sens}, considering fixed values of (a) χ and (b) φ (or, equivalently, the corresponding combinations of N and r_s). In both cases, the performance without overlapped sensed areas (w/o ov, simulations) and that with overlapped sensed areas (w ov, analysis) are shown.

the case (a) can be carried out: more precisely, the smaller the value of β_{sens}, the closer the performance predicted by the analytical framework (no overlap) is to that with random node deployment (overlap). Note, however, that for $\beta_{\text{sens}} = 1$ the probability of missed detection does not depend on the value of φ, in agreement with the results in Fig. 5(b).

To summarize, by comparing the results presented in Fig. 5 with those in Fig. 6, it can be concluded that:

- when $\beta_{\text{sens}} = 1$, the probability of missed detection predicted by the analytical framework in Section 4.1, based on the assumption of non-overlapped sensed areas, is optimistic with respect to that in a scenario with random node deployment;
- when $\beta_{\text{sens}} < 1$, the probability of missed detection predicted by the analytical framework accurately estimates that, evaluated through simulations, relative to the case of random node deployment.

4.3.3. Non-linear trajectories

In the derivation of the analytical framework and in all results previously presented, linear target trajectories have been considered. However, from a realistic point of view, it is likely that a target may change its trajectory after entering the monitored area, e.g., because of terrain morphology. Therefore, it is of interest to understand the impact of non-linear target trajectories on the system performance. As the analytical framework is based on the assumption that all possible trajectories are equally likely, we intuitively expect that it will remain approximately valid also in the presence of non-linear trajectories.

In order to validate the previous assertion, we evaluate the probability of missed detection in the case that the target, after entering the monitored area along a linear trajectory, changes (only one time) its direction of movement by an angle uniformly distributed in $(0, 2\pi]$ after a time interval uniformly distributed in $(0, t_{\text{traj}}]$, where $t_{\text{traj}} \ll d_s/v = 66.7$ s (d_s/v s is the time required for the target to cross a side of the monitored area). In particular, we consider $t_{\text{traj}} = 20$ s. In Fig. 7, the probability of missed detection is shown, as a function of β_{sens}, in the presence of linear (dashed lines) and non-linear (solid lines) trajectories. In all cases, pseudo-random node deployment without overlapping between the sensed areas is considered: the performance with linear trajectories is obtained with the proposed analytical framework, whereas the performance with non-linear trajectories is obtained by means of computer simulations. The obtained results confirm the intuitive prediction that the impact of possible trajectory changes is very limited. Indeed, since there is no information about the entrance point and the entrance angle of a target, a trajectory change is roughly equivalent to considering a different trajectory, and this has no impact, from a statistical point of view, on the performance. We also point out that if a trajectory change occurs within a sensed area, the length of the intersection between the target trajectory and the sensed area may be higher than that without trajectory change.

4.4. Extension to multiple-target detection scenario

While all results presented so far refer to scenarios with a single incoming target, in the case of multiple-target intrusion, the operator could be interested in knowing either the probability of missing all targets or the probability of missing at least one of the incoming targets. In the remainder of this subsection, we consider a multiple-target detection scenario where several targets enter the surveillance area from various entrance points at the same time. We first derive the probability of missing all incoming targets, referred to as P_{ma}. Due to the independence of the incoming targets, it immediately follows that

$$P_{\text{ma}} = (P_{\text{md}})^{N_T} \tag{9}$$

where P_{md} is the probability of missed detection in the presence of a single target, and N_T is the number of targets entering simultaneously the monitored area. P_a thus represents the probability of remaining totally unaware of the incoming threat. Conversely, $1 - P_{\text{ma}}$ indicates the probability of detecting at least one target among the group of N_T intruders.

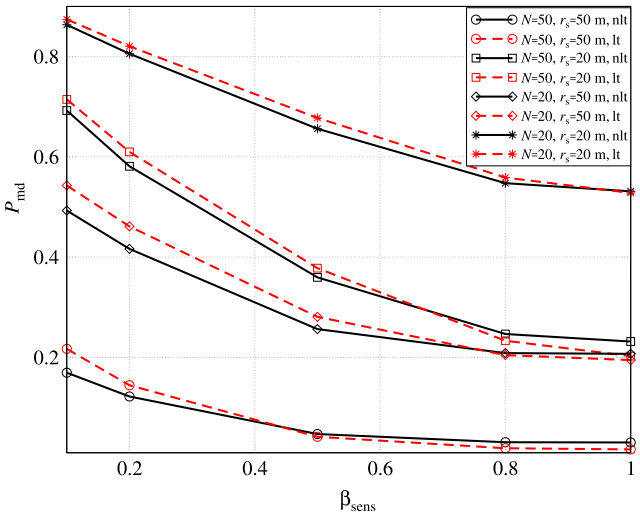

Fig. 7. Probability of missed detection, as a function of β_{sens}, with pseudo-random node deployment without sensed areas' overlapping. The performance with target linear (lt) and non-linear (nlt) trajectories is analyzed through the analytical framework and simulations, respectively. Different values of N and r_s are considered.

We now derive the probability of missing at least one out of the N_T incoming targets, referred to as P_{mo}. Since the complementary event corresponds to detecting each incoming target, P_{mo} can be expressed as follows:

$$P_{\text{mo}} = 1 - (1 - P_{\text{md}})^{N_T}. \tag{10}$$

By using the analytical lower bound (8) on P_{md}, it is straightforward to derive lower bounds for P_{ma} and P_{mo}.

From (9) and in (10), it is immediate to conclude that an error on the estimation of P_{md} leads to errors on the estimation of P_{ma} and P_{mo}. According to the error propagation law [30], the error δ_z on a function $z = z(x_1, \ldots, x_N)$ can be expressed as

$$\delta_z = \sum_{i=1}^{N} \frac{\partial z}{\partial x_i} \mathrm{d}x_i. \tag{11}$$

Applying (11) to (9), one obtains:

$$\frac{\delta_{P_{\text{ma}}}}{P_{\text{ma}}} = N_T \frac{\delta_{P_{\text{md}}}}{P_{\text{md}}} \tag{12}$$

where $\delta_{P_{\text{ma}}}$ is the error on the estimation of P_{ma} and δ_{Pmd} is the error on the estimation of P_{md}. Similarly, one can express the error $\delta_{P_{\text{mo}}}$ on the estimation of P_{mo} as

$$\frac{\delta_{P_{\text{mo}}}}{P_{\text{mo}}} = N_T \frac{\delta_{P_{\text{mo}}}}{1 - P_{\text{md}}}. \tag{13}$$

From (12) and in (13), one concludes that the errors on the estimation of P_{ma} and P_{mo} depend linearly on the number incoming targets. Therefore, for a given estimation error on P_{md} (single target), the larger is the number of simultaneously incoming targets, the worse are the estimation accuracies of P_{ma} and P_{mo}. This will be confirmed by the following results.

In Fig. 8(a), P_{ma} is shown, as a function of β_{sens}, considering various values (namely 2 and 4) of the number N_T of targets entering the monitored area at the same time. The targets enter with speed $v = 15$ m/s into the monitored area with side $d_s = 1000$ m, where $N = 50$ sensors with sensed range equal to $r_s = 50$ m are randomly deployed. For each value of N_T, simulation (solid lines) and theoretical (dashed lines) results are compared. In the simulations, it is assumed that a single sensor can simultaneously detect, when active, multiple targets crossing its sensed area at the same time. In all cases (both analysis and simulation), we assume a pseudo-random node deployment without overlapped sensed areas. As intuition may suggest, the probability of missing all incoming targets is lower than P_{md}. This effect is more and more pronounced when the number of incoming targets increases. As an asymptotic effect, P_{ma} tends to zero. On the other hand, decreasing the value of β_{sens} yields a higher value of P_{ma}, since the awareness of the nodes is reduced. In Fig. 8(b), P_{mo} is shown, as a function of β_{sens}, considering three possible values (2, 4, 8) for N_T. As before, in each scenario simulation (solid lines) and analytical (dashed lines) results are shown. As the intuition suggests, when the number of targets increases, it is more and more likely that at least one target can cross the monitored area without being detected by the system. As shown in Fig. 4(a) for a single-target case, in the absence of clustering simulation and analytical results present a small discrepancy. Considering Fig. 8(b), it can be concluded that this discrepancy is amplified in the presence of multiple targets.

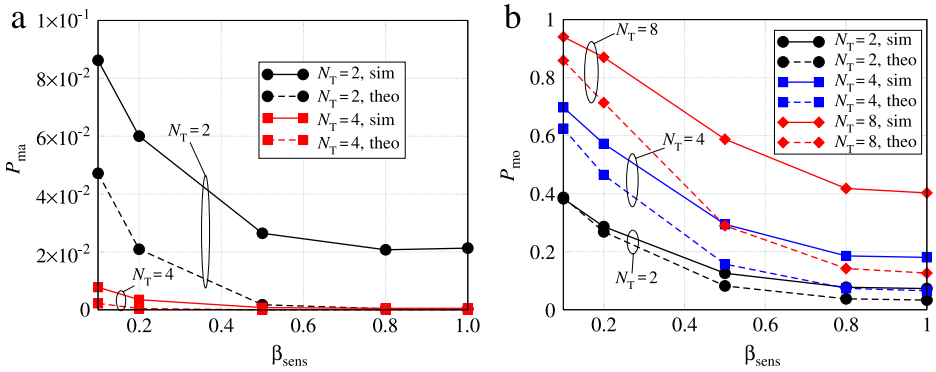

Fig. 8. Simulation (solid lines) and analytical (dashed lines) results for (a) the probability of missing all the incoming targets and (b) the probability of missing at least one of the incoming targets, as functions of the duty cycle β_{sens}. In all cases, pseudo-random node deployment without overlapped sensed areas is assumed.

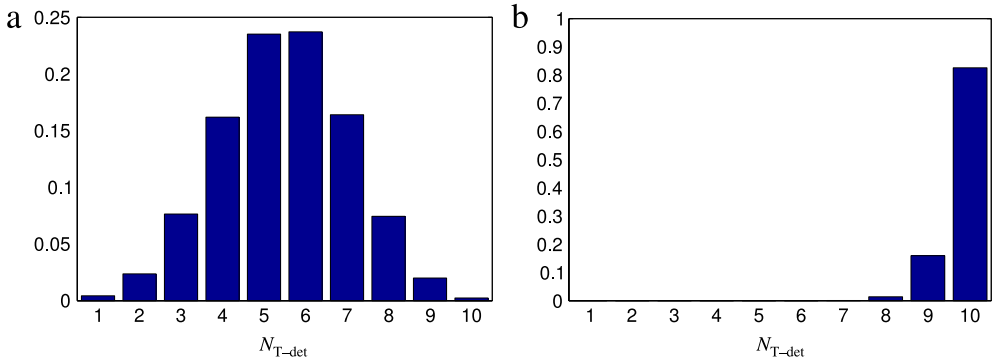

Fig. 9. PMF of the number N_{T-det} of detected targets, out of the $N_T = 10$ incoming targets, considering (a) $N = 10$ and (b) $N = 50$ deployed nodes. The duty cycle is $\beta_{sens} = 0.8$.

In order to evaluate the target detection capabilities of the WSN, we analyze the probability of detecting exactly N_{T-det} out of the N_T simultaneously incoming targets. Since the targets are independent, the probability mass function (PMF) of N_{T-det} is binomial with parameters N_T and $(1 - P_{md})$, i.e.:

$$P\{N_{T-det} = n\} = \binom{N_T}{n} (1 - P_{md})^n P_{md}^{(N_T - n)} \quad n = 0, \ldots, N_T.$$

The PMF of N_{T-det} is shown in Fig. 9(a) and (b), considering $N = 10$ and $N = 50$ deployed nodes, respectively. In both cases, $N_T = 10$ targets. All the other network parameters are set as in Fig. 8. The duty cycle is set to $\beta_{sens} = 0.8$. In particular, since N_T has a binomial distribution, the average number of detected target is $\eta_{T-det} = N_T(1 - P_{md})$. In the case with $N = 10$ nodes, shown in Fig. 9(a), the system has limited detection capabilities, due to the limited number of deployed nodes. More precisely, $\eta_{T-det} = 5.47$, i.e., the system can detect, on average, half of the incoming targets. In the case with $N = 50$ nodes, shown in Fig. 9(b), the system can detect almost all incoming targets. In this case, in fact, $\eta_{T-det} = 9.81$, i.e., on average, 98% of the targets is detected.

According to the analytical framework presented in this section, it is then possible to evaluate (for a given scenario, i.e., given value of P_{md}) the average number of detected target η_{T-det} as a function of the number of simultaneously incoming target N_T. In Fig. 10, we analyze the impact of the duty cycle β_{sens} on η_{T-det}. In the considered scenario, $N = 50$, and the other parameters are set as in Fig. 8. In the same figure, the reference curve for the ideal case (i.e., all targets are detected) is also shown as a dotted line. In the case with $\beta_{sens} = 0.8$, the target detection performance remains close to the ideal one, i.e., all incoming targets are, on average, detected. When β_{sens} reduces to 0.1, an expected performance degradation can be observed.

On the basis of the extension presented in this subsection, the following considerations can be carried out. Given the network configuration and the number of incoming targets, it is possible to predict the system performance (in terms of average number of detected targets) or, conversely, configure the network in order to meet the desired goal in terms of detection performance.

5. Delay for detection

In order to complement the framework presented in the previous section, it is of interest to compute the average delay between the target entrance instant and the instant of the first detection by a sensor. As for the derivation of the

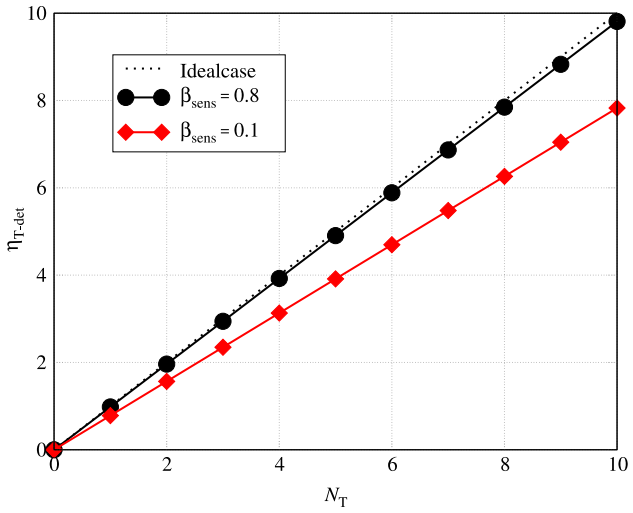

Fig. 10. Average number of detected targets as a function of the number of simultaneously incoming targets, considering two different values of β_{sens}.

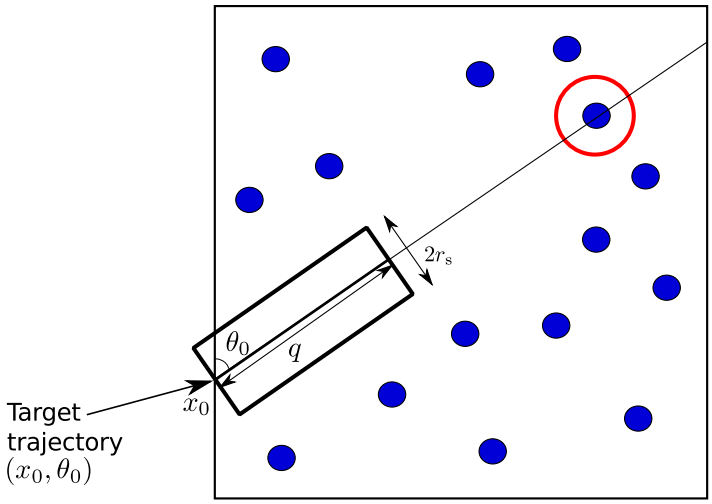

Fig. 11. Illustrative example of a target traveling for a distance q without being detected by any sensor in the network.

probability of missed detection, we build on the derivation presented in [6], carried out in the absence of duty cycle for homogeneous planar Poisson distributed nodes. We remark that the Poisson node distribution is representative of a random node deployment.

Let us first compute the probability that no sensor is met by a target on its path. Note that a target is detected by a sensor if the distance of its trajectory from the sensor is shorter than r_s.[4] Referring to the illustrative scenario in Fig. 11, the probability that a target is not detected along a path of length q can be accurately approximated with the probability that no sensor lies in the rectangle, of area $2r_s q$, shown in Fig. 11 (the rectangle is centered on the path). In other words, one can the express the probability that the length of the free (from detection) path, denoted as Q, is larger than q as:

$$P(Q > q) = \left(1 - \frac{2r_s q}{d_s^2}\right)^N. \tag{14}$$

The average length of the free path can then be evaluated as follows:

$$\begin{aligned}\mathbb{E}[Q] &= \int_0^{\bar{q}_{\max}} P(Q > q)\mathrm{d}q = \int_0^{\bar{q}_{\max}} \left(1 - \frac{2r_s q}{d_s^2}\right)^N \mathrm{d}q \\ &= \frac{d_s^{2(N+1)} - (d_s^2 - 2\bar{q}_{\max} r_s)^{N+1} d_s^{-2N}}{2r_s(N+1)}\end{aligned} \tag{15}$$

where $\bar{q}_{\max}$ is the average maximum length of a target trajectory inside the monitored area. In particular, the maximum length $q_{\max}$ (i.e., the length of the portion of the trajectory within the monitored area) depends on both the entrance point

[4] This is true since the sensors are preliminary assumed always on. Later on, this assumption will be relaxed.

x_0 and the entrance angle θ_0 of the target, as shown in Fig. 11. In particular, it is possible to express the value $q_{\max}$ as the following function of (x_0, θ_0):

$$q_{\max}(x_0, \theta_0) = \begin{cases} \dfrac{d_s - x_0}{\cos(\theta_0)} & 0 < \theta_0 < \operatorname{atan}\left(\dfrac{d_s}{d_s - x_0}\right) \\ \dfrac{d_s}{\sin(\theta_0)} & \operatorname{atan}\left(\dfrac{d_s}{d_s - x_0}\right) < \theta_0 < \operatorname{atan}\left(\dfrac{x_0}{d_s}\right) + \dfrac{\pi}{2} \\ -\dfrac{x_0}{\cos(\theta_0)} & \operatorname{atan}\left(\dfrac{x_0}{d_s}\right) + \dfrac{\pi}{2} < \theta_0 < \pi. \end{cases} \tag{16}$$

The three cases presented in (16) come from geometrical considerations. In fact, due to the square shape of the monitored surface, it is not possible to express the length of $q_{\max}$ with a single closed-form equation. For instance, assuming that the target enters from the side on the bottom, the three cases depends on whether the target trajectory exits from the side on the left, on the top or on the right, respectively. For symmetry reasons, similar considerations hold when the target enters from other sides. The average maximum length can be finally computed as

$$\bar{q}_{\max} \triangleq \int_{\mathcal{D}_{X_0}} \int_{\mathcal{D}_{\Theta_0}} q(x_0, \theta_0) f_{X_0,\Theta_0}(x_0, \theta_0) \mathrm{d}x_0 \mathrm{d}\theta_0 \tag{17}$$

where $f_{X_0,\Theta_0}(x_0, \theta_0) = f_{X_0}(x_0) f_{\Theta_0}(\theta_0)$ (owing to the independence between the entrance point and the entrance angle), $f_{X_0}(x_0) \sim \mathrm{Unif}[0, d_s]$ $\left(\mathcal{D}_{x_0} = [0, d_s]\right)$, and $f_{\Theta_0}(\theta_0) \sim \mathrm{Unif}[0, \pi]$ $\left(\mathcal{D}_{\theta_0} = [0, \pi]\right)$. As the integral at the right-hand side of (17) does not have a closed-form solution, it has to be evaluated numerically. The obtained value of $\bar{q}_{\max}$ can be inserted into (15) and, finally, $\mathbb{E}[Q]$ can be evaluated.

If the sensing devices are always on, then given the target speed v and the length of the free path, the delay for detection can be immediately evaluated as $D_{\mathrm{det}} = \mathbb{E}[Q]/v$. If sensing duty cycle is introduced, the previous derivation must be refined to take into account the case where some sensors lie inside the rectangle of area $2qr_s$, but they cannot detect the target since their sensing devices are off. Therefore, the probability that no sensor detects the target after it has traveled over a path of length q can be rewritten as

$$P(Q > q) = \left(1 - \frac{2qr_s}{d_s^2}\right)^N + \sum_{i=1}^{N} P\{\mathcal{A}_i\} \tag{18}$$

where $\mathcal{A}_i \triangleq$ {There are i nodes inside the rectangle and their sensing ranges are off} and the first term at the right-hand side of (18) represents the probability that no node lies inside the rectangle of area $2qr_s$ (and corresponds to (14)). According to the derivation presented in Section 4.2, $P\{\mathcal{A}_i\}$ can be expressed as

$$P\{\mathcal{A}_i\} = \binom{N}{i} \left(1 - \frac{2qr_s}{d_s^2}\right)^{N-i} \left(\frac{2qr_s}{d_s^2} P\{\mathcal{E}_{\mathrm{SoT}}, \bar{\mathcal{E}}_{\mathrm{det}}\}\right)^i \tag{19}$$

where $P\{\mathcal{E}_{\mathrm{SoT}}, \bar{\mathcal{E}}_{\mathrm{det}}\} = (1 - P\{\mathcal{E}_{\mathrm{det}} | \mathcal{E}_{\mathrm{SoT}}\}) P\{\mathcal{E}_{\mathrm{SoT}}\}$ is the probability that the target trajectory crosses the area sensed by a node and this node does not detect the target. By inserting (19) in (18), $\mathbb{E}[Q]$ can then be numerically evaluated as in (15), where $\bar{q}_{\max}$ has the expression given by (17). Then, D_{det} can be immediately computed.

In Fig. 12, D_{det} is shown as a function of the sensing duty cycle, considering scenarios where various numbers of sensors are deployed over the monitored area. For small values of N, it can be observed that the analytical model is relatively coarse, especially for small values of β_{sens}. However, even in this case the gap between simulation and analytical results is limited. When the number of deployed nodes increases ($N \geq 50$), the accuracy of the analytical model becomes very high.

6. Latency after detection

When a target is detected, the time the alert takes to reach the sink has to be as short as possible. In the following, we first derive the per-hop latency, denoted as $D_{1\,\mathrm{hop}}$, and then compute the latency over a multi-hop path. We verify the validity of our model with experimental measurements on a Crossbow MicaZ testbed [25].

As introduced in Section 3.2, the transmission latency is evaluated considering the off-the-shelf X-MAC protocol, i.e., a low-power asynchronous MAC-layer protocol for duty-cycled WSNs [27]. The X-MAC protocol uses Low-Power Listening (LPL), or preamble sampling, to enable low-power communications between a sender and a receiver. X-MAC does not synchronize wake-up and sleep schedules of nodes. Senders uses a preamble at least as long as the sleeping interval of the receiver. This guarantees that the receiver will wake up, detect the preamble, and stay awake for the reception of the data. The X-MAC protocol uses a strobed preambling approach in which the sender quickly alternates between sending the packet destination address and waiting a short time, so that the receiver can potentially abort the process to start receiving data. This approach allows to further reduce energy consumption and per-hop latency in comparison with protocols using long preambles, such as B-MAC [31].

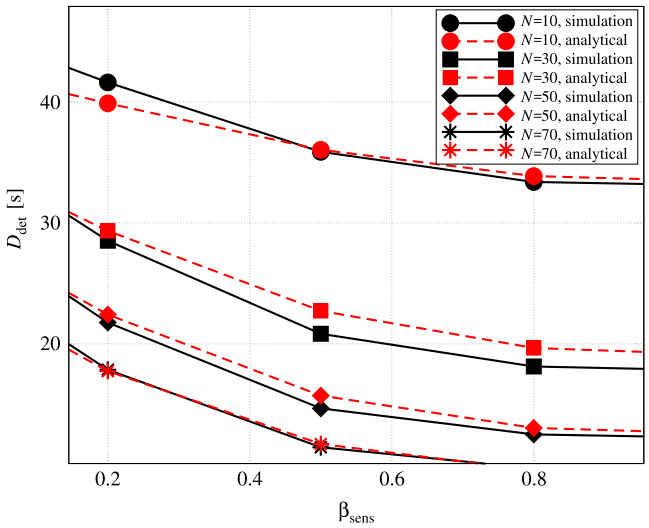

Fig. 12. Simulation (solid lines) and analytical (dashed lines) D_{det} results as functions of β_{sens}, considering different number of nodes.

The average per-hop transmission latency for the X-MAC protocol can be expressed as follows:

$$D_{1\,\text{hop}} = \frac{(1-\beta_{\text{comm}})^2 t_{\text{comm}}}{2} + S_{\text{p}} + S_{\text{al}} + S_{\text{d}} \tag{20}$$

where β_{comm} is the (normalized) communication duty cycle over the period t_{comm}, and S_{p}, S_{al}, and S_{d} are the durations (dimension: [s]) of the strobed preamble, the preamble ack message, and the alert packet, respectively. We now explain the rationale behind (20). Considering the status of the receiving node, i.e., if the communication subsystem is either turned on or off, the probability that a node begins its transmission when the receiving node is on is β_{comm} and the associated latency is $S_{\text{p}} + S_{\text{al}} + S_{\text{d}}$. On the other hand, the probability that a node is off is $1 - \beta_{\text{comm}}$. We evaluate $D_{1\,\text{hop}}$ simply as the arithmetic average between the worst and best cases. The best case is when a node starts transmitting exactly when the receiving node starts its LPL operations, so that the packet is transmitted after $S_{\text{p}} + S_{\text{al}} + S_{\text{d}}$. In the worst case, the transmitting node waits for the entire duration of the sleeping interval. In addition, since the receiving node must receive an entire preamble before sending the ack message, the worst case takes into account that two transmissions of the preamble may be required in order to start the communication. In this case, the latency introduced by the transmission is $(1 - \beta_{\text{comm}})t_{\text{comm}} + (S_{\text{p}} + S_{\text{al}}) + S_{\text{d}}$. By (i) scaling this term by the probability that the receiver is off, (ii) averaging the best and the worst cases, and (iii) adding the latency related to the case with the receiver on and scaled by its probability of being on, expression (20) for $D_{1\,\text{hop}}$ can be obtained.

Considering a multi-hop path, the average global latency can be simply expressed as $D = D_{1\,\text{hop}} N_{\text{hop}}$, where N_{hop} denotes the average number of nodes that the alert message traverses to reach the sink. The processing time at the relaying nodes is neglected.

In order to verify the analytical model of the multi-hop alert transmission latency, we have run a set of experimental tests with a testbed of 4 Crossbow MicaZ nodes deployed in a chain topology. The first node injects a packet every 2 s. Each subsequent node forwards the packet to its neighbor until it reaches the last node, which reverses the transmission direction. We have measured the round-trip time setting N_{hop} from 2 to 6, and β_{comm} to either 0.067, 0.1 or 0.2.[5] For each pair of values, we compute the average latency as the mean round-trip time of 100 samples, along with the 95% confidence interval. In Fig. 13, a comparison between theoretical and experimental results is shown. The curves are quite close, even though a gap appears when β_{comm} becomes lower and the duration of the sleeping interval increases. This may be due to the unavoidable alignment of sleep schedules on the packet's way back, which tends to reduce the latency for large values of sleeping interval durations, i.e., small values of β_{comm}. In the context of the reference scenario, the experiments show the validity of the analytical model, i.e., the latency is well approximated as $D \simeq N_{\text{hop}}(1 - \beta_{\text{comm}})t_{\text{comm}}/2$.

Note that the proposed derivation relies on the assumption of collision-free transmission of the alert. This is realistic for a single-target scenario with low arrival rate and in the presence of partial node coverage (as considered in this work). Indeed, in all considered scenarios there is an order of magnitude of difference between the average times (i) for a target to transit from one sensed area to another and (ii) for an alert notification to reach the sink. In fact, the average distance between neighboring nodes is on the order of $1/\sqrt{\rho_{\text{s}}}$ [32], where $\rho_{\text{s}} = N/d_{\text{s}}^2$ is the node spatial density. Therefore, the shortest time[6] required to transit from the border of a sensed area to the border of a neighboring sensed area, denoted as t_{transit},

[5] These values of β_{comm} correspond to a static active period of 8 ms and t_{comm} equal to 120 ms, 80 ms and 40 ms, respectively.

[6] This time is observed when the target moves along the line connecting the centers of the neighboring sensed areas.

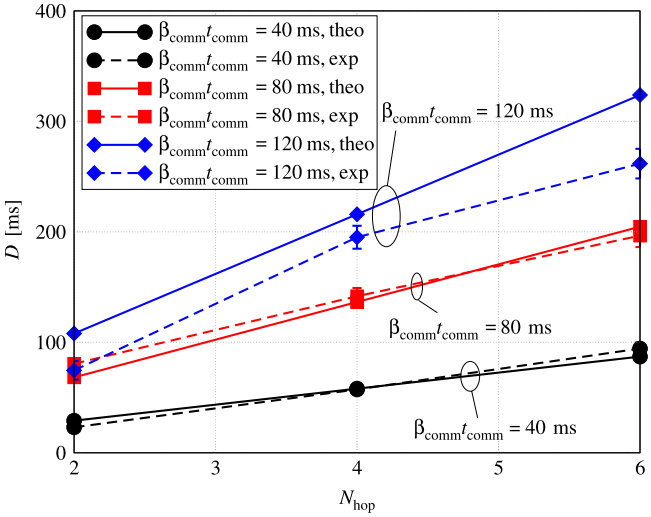

Fig. 13. Latency as a function of the number of hops traversed by a packet. Both (i) experimental (dashed lines) and (ii) theoretical results (solid lines) are presented.

can be expressed as follows:

$$t_{\text{transit}} = \frac{1/\sqrt{\rho_s} - 2r_s}{v}.$$

Considering reference system parameter values ($N = 50$, $d_s = 1000$ m, $r_s = 50$ m, and $v = 15$ m/s), it follows that $t_{\text{transit}} \simeq 2.8$ s. In the case of $N_{\text{hop}} = 3$ with $\beta_{\text{comm}} = 6.6\%$, from Fig. 13 it follows that $D \simeq 136$ ms. Therefore, $D \ll t_{\text{transit}}$. In other words, an alert notification sent by a sensor node will very likely reach the sink far before the target will be detected by another sensor. In the presence of multiple concurrent senders, the X-MAC protocol features contention-avoidance mechanisms to keep the latency low and the throughput high. To take into account this mechanisms, even if contention might not occur frequently in our case, further refinements of the model would be required.

7. Average network lifetime

As nodes operate on batteries, the way they consume energy has a direct impact on the lifetime of the surveillance system. To take this into account, we now propose a simple energy model for the engineering toolbox.

The energy consumption of a node can be roughly estimated as the sum of the energies consumed by its hardware components. For the sake of simplicity, we only integrate in the energy model contributions from the sensing sub-unit and the communication sub-unit (radio transceiver). The network lifetime is defined as the time needed for the average residual energy E_r to be lower than a (given) threshold value E_{th}, which can be used to model the physical behavior of a node. The average residual energy at time t, denoted as $E_r(t)$, can be expressed as

$$E_r(t) = NE_i - N\Omega_{\text{tot}}t \tag{21}$$

where E_i is the initial energy of a node and Ω_{tot} (dimension: [W]) is the total power consumed by sensing and communication operations (assumed to be time-invariant). According to the description of the X-MAC protocol in Section 6, there are four possible states for a node: (i) transmission, (ii) reception, (iii) sleep, and (iv) LPL, with corresponding power consumptions denoted as Ω_T, Ω_R, Ω_s, and Ω_{LPL} (dimension: [W]), respectively. Ω_{tot} in (21) can then be computed as follows:

$$\Omega_{\text{tot}} = \Omega_{\text{sensing}} + \Omega_{\text{LPL}} + (\Omega_R + \Omega_T)P_d N_{\text{target}}$$

where: Ω_{sensing} is the power consumption associated with the sensing device in the activity period of duration t_{sens}; Ω_{LPL} is the power required when performing the LPL operations (over a period of duration t_{comm}); Ω_R is the power used by a node to receive a packet; Ω_T is the power used to transmit an alert packet; P_d is the target detection probability; and N_{target} is the number of times that a target appears during a reference period. The average power to transmit an alert packet can then be expressed as

$$\Omega_T = \left[\Omega_{\text{Tx}}S_d + \frac{(1-\beta_{\text{comm}})t_{\text{comm}}}{2(S_p + S_{\text{al}})}(\Omega_{\text{Tx}}S_p + \Omega_{\text{Rx}}S_{\text{al}})\right]\frac{N_{\text{hop}}}{Nt_{\text{comm}}} \tag{22}$$

where the first additive term in the squared brackets, i.e., $\Omega_{\text{Tx}}S_d$, is the energy spent to transmit the data portion of the packet, whereas the second additive term corresponds to the energy consumption due to the periodic preamble transmission in order to notify the receiving node of a packet arrival. As in Section 6, since nodes are not synchronized, we assume that the average number of preamble transmissions is the arithmetic average between best and worst cases. The term N_{hop}/N is introduced owing to the fact that only a subset of the N sensors is used to relay the alert message to the AP.

The average power to receive a packet can be expressed as

$$\Omega_{\mathrm{R}} = \frac{[\Omega_{\mathrm{Rx}} S_{\mathrm{d}} + (\Omega_{\mathrm{Rx}} S_{\mathrm{p}} + \Omega_{\mathrm{Tx}} S_{\mathrm{al}})]}{t_{\mathrm{comm}}} \frac{N_{\mathrm{hop}}}{N} \tag{23}$$

where $\Omega_{\mathrm{Rx}} S_{\mathrm{d}}$ is the energy spent to receive a packet and $\Omega_{\mathrm{Rx}} S_{\mathrm{p}} + \Omega_{\mathrm{Tx}} S_{\mathrm{al}}$ is the energy spent for the reception of the preamble and the transmission of the ack message. Since in the scenario considered there is no information about the position of the AP, the average number of hops has been determined by calculating, using the Dijkstra algorithm [33], the shortest path from each node to every other node in the network. Given that the transmission range r_{T} is around 250 m and $N = 50$ nodes are deployed within the monitored area, the estimated value of N_{hop}, heuristically evaluated through simulations, is around 2.7, which being N_{hop} an integer value, is rounded to 3.

The power associated with the LPL operations can be expressed as

$$\Omega_{\mathrm{LPL}} = \Omega_{\mathrm{Rx}} \beta_{\mathrm{comm}} + \Omega_{\mathrm{s}} (1 - \beta_{\mathrm{comm}}) - \Gamma_{\mathrm{Tx}} - \Gamma_{\mathrm{Rx}} \tag{24}$$

where Γ_{Tx} and Γ_{Rx} are two corrective terms, described in more detail below. In particular, the powers in (22)–(24) are evaluated considering the energies consumed over a period of duration t_{comm}. However, during normal operations the node either performs LPL operations or transmits/receives a packet. Γ_{Tx} and Γ_{Rx} are used to refine the power consumption due to LPL operations. In fact, the LPL and also the transmission and reception intervals overlap for short intervals, so that without these two terms the power consumption budget would be higher than the correct one. In particular, Γ_{Tx} can be expressed as

$$\Gamma_{\mathrm{Tx}} = \left\{ \Omega_{\mathrm{s}} \left[\frac{(1 - \beta_{\mathrm{comm}}) t_{\mathrm{comm}}}{2} + S_{\mathrm{d}} + S_{\mathrm{al}} \right] + \Omega_{\mathrm{Rx}} S_{\mathrm{p}} \right\} P_{\mathrm{d}} N_{\mathrm{target}} \frac{N_{\mathrm{hop}}}{N t_{\mathrm{comm}}} \tag{25}$$

whereas Γ_{Rx} can be expressed as

$$\Gamma_{\mathrm{Rx}} = \left[(S_{\mathrm{al}} + S_{\mathrm{d}})\, \Omega_{\mathrm{s}} + \Omega_{\mathrm{Rx}} S_{\mathrm{p}} \right] P_{\mathrm{d}} N_{\mathrm{target}} \frac{N_{\mathrm{hop}}}{N t_{\mathrm{comm}}}. \tag{26}$$

The term Γ_{Tx} takes into account the fact that, during transmission operations, such as (i) periodic preamble transmission over an interval of duration $(1 - \beta_{\mathrm{comm}}) t_{\mathrm{comm}}/2$, (ii) packet transmission, and (iii) acknowledgment reception, a node would normally be in the sleep state, whereas during the transmission of the preamble, that will be acknowledged by the receiving node, a node would normally be in the reception state. Thus, the correction factor Γ_{Tx} is necessary, since otherwise the energy consumed by the node with this model would be higher than the real value because reception and transmission operations would overlap with normal LPL operations for a period. Similar considerations can be carried out for the term Γ_{Rx}. In fact, when a node is waiting for the acknowledgment window to transmit an ack message, to receive the preamble, and to transmit a packet (according to the LPL operations), it would normally be in the sleep state. The same considerations come into play when a node is receiving the preamble, since it would normally be in the receiving state for the LPL operations.

Finally, the power consumed during sensing operations can be expressed as

$$\Omega_{\mathrm{sensing}} = \beta_{\mathrm{sens}} \Omega_{\mathrm{sens}} \tag{27}$$

where Ω_{sens} is the power consumption for sensing operations.

Introducing the expressions (25) and (26) into (24) and the expressions (22), (23), (24) and (27) into (21), it is possible to derive an expression for the energy consumption which depends on both sensing and communication parameters.

The network lifetime $\mathcal{L}$ is the time at which $E_{\mathrm{r}}(\mathcal{L}) = E_{\mathrm{th}}$ and, from (21) one obtains:

$$\mathcal{L} = \frac{N E_{\mathrm{i}} - E_{\mathrm{th}}}{N \Omega_{\mathrm{tot}}}. \tag{28}$$

8. System engineering: an application case

In this section, we study a use case where a surveillance system has to be optimally configured to maximize the network sustainability, i.e., its lifetime $\mathcal{L}$, and for given quality of service requirements in terms of probability of missed detection (P_{md}) and latency for alert transmission to the AP (D). Since Eqs. (8) and (28) are not linear, standard linear programming optimization techniques cannot be used. However, the three equations form a convex set, which makes gradient-based optimization techniques feasible [34]. Throughout this section, the target arrival rate N_{target} is fixed at 10 targets per day.

A realistic use case of the proposed framework is the maximization of the lifetime $\mathcal{L}$ of the WSN under the constraint of given maximum values of D and P_{md}, denoted as D^* and P^*_{md}, respectively. This application case consists of the optimization of a single-objective function, given constraints on the two other functions. The optimal parameters can be evaluated using single-objective convex programming techniques. In Fig. 14, the longest lifetime ($\mathcal{L}_{\max}$), under the constraints $P_{\mathrm{md}} < P^*_{\mathrm{md}}$ and $D < D^*$, is shown as a function of P^*_{md} and D^*.

In particular, for a given pair of values of D^* and P^*_{md}, we evaluate the longest lifetime that can be achieved. Of course, the more stringent the requirements on D and P_{md}, the shorter the achievable lifetime. In fact, for small values of P^*_{md} and D^*, a

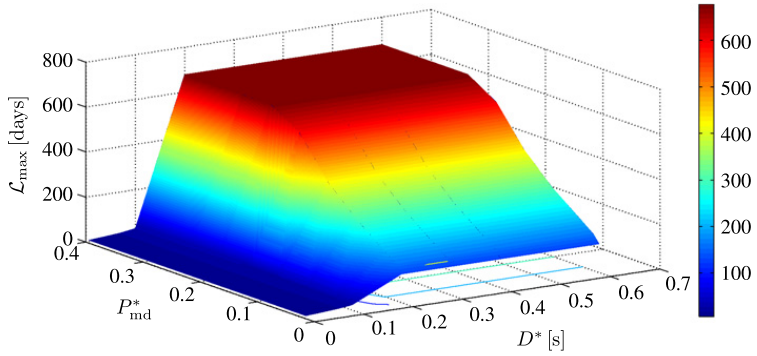

Fig. 14. Longest achievable lifetime ($\mathcal{L}_{\max}$) under probability of missed detection (P^*_{md}) and latency (D^*) constraints.

sensor must keep its sensing interface on (to minimize P_{md} and D) and its communication interface on (to minimize D) for a large portion of each sensing/communication period, so that the energy consumption increases and the lifetime shortens. On the other hand, when the requirements are less stringent, the sensing and communication interfaces can be switched off for a longer portion of the period, and, consequently, the lifetime becomes larger.

Focusing on the shape of the surface, generated by interpolation of the simulation results, it is possible to understand the contribution of both sensing and communication operations. When the latency requirements are stringent, the lifetime is short. Obviously, if the latency requirements are relaxed, the lifetime increases towards a saturation value which depends on P^*_{md}. A short latency corresponds to a short network lifetime, since (i) the power consumed during reception is several orders of magnitude larger than the power consumed in the sleep phase and (ii) the communication interface of each node must be on for a large portion of the communication period t_{comm} in order to ensure that a packet is delivered to the AP in a short time. The impact of the latency on $\mathcal{L}_{\max}$ becomes negligible, i.e., the lifetime saturates, with respect to D^*, when $D^* \simeq 0.15$ s. In fact, this value corresponds to the minimum allowed value of β_{comm} that guarantees that a preamble is correctly received in order for a communication to start. Therefore, larger values of D^* have no impact on the latency, since lower values of β_{comm} cannot be selected.

Focusing on the $P^*_{\mathrm{md}} - \mathcal{L}_{\max}$ plane, it turns out that the power consumption during sensing is basically negligible when the latency requirements are limited. In fact, the power consumption associated with sensing operations is one order of magnitude lower than that related to reception operations. When the maximum tolerable latency becomes longer than 0.15 s, the power consumption related to the communication interface remains constant and the lifetime is affected only by the sensing power consumption. In this case, the lower P^*_{md} (i.e., the more stringent the constraint on the probability of missed detection), the higher the energy consumption, since a sensor must be on for a longer interval.

9. Concluding remarks

This paper has addressed the problem of energy-efficient target detection using unattended WSNs. We have first derived a framework for the evaluation of various performance indicators that are useful for the characterization of a WSN-based surveillance application, under the assumption of random node deployment. In particular, the proposed framework allows to evaluate the probability of missed detection of one or multiple incoming targets, the delay for detecting a target, the latency of notification transmission, and the network lifetime. By leveraging on this "toolbox", we have then characterized the trade-offs faced by WSNs with respect to energy consumption and quality of service, in terms of detection capabilities and latency. This toolbox allows to optimally configure a given WSN for a variety of quality of service performance indicator requirements. As such, the engineered toolkit gives the possibility to an operator to set up efficiently an unattended WSN for a wide range of scenarios like counting applications with poor latency requirements (e.g., counting animals in a given area using passive infra-red sensing), as well as live monitoring applications with a strong latency D and medium P_{md} requirements (e.g., tracking emergency or panic situations in a public subway, using audio sensing) or application with strong delay for detection D_{det} requirements (e.g., access detection in sensible areas using seismic sensors).

Further works along these lines include extensions of the engineering toolbox to encompass (i) deterministic node deployment, addressing, for instance, physical constraints imposed by the surface morphology, (ii) non-ideal sensing and transmission ranges, using multiple sensing modalities, (iii) coordinated sensing activities, and (iv) exhaustive energy models for complex sensor nodes, in order to improve the overall accuracy with respect to real operating conditions. We also envision to assess the performance of simple target detection applications, using the open large-scale WSN testbed provided by the French national project SensLab, with specific WSN architectures such as those presented in [35].

Acknowledgements

The authors would like to thank the two anonymous reviewers for their insightful observations.

The largest part of the first author's work was carried out when he was visiting Thales Communications (2009) and when he was at the University of Parma (2010).

References

[1] E. Yanmaz, H. Guclu, Stationary and mobile target detection using mobile wireless sensor networks, in: Proc. of 28th IEEE Conf. on Computer Communications, INFOCOM 10, San Diego, CA, 2010.
[2] V. Prasad, T. Yan, P. Jayach, Z. Li, S.H. Son, J.A. Stankovic, J. Hansson, T. Abdelzaher, Andes: an analysis-based design tool for wireless sensor networks, in: Proc. of 28th IEEE Real-Time Systems Symposium, RTSS 07, Tucson, AZ, 2007.
[3] J. Jeong, Y. Gu, T. He, D. Du, VISA: virtual scanning algorithm for dynamic protection of road networks, in: Proc. of 28th IEEE Conf. on Computer Communications, INFOCOM 09, Rio de Janeiro, Brazil, 2009.
[4] H. Zhang, J. Hou, Maintaining sensing coverage and connectivity in large sensor networks, Ad Hoc & Sensor Wireless Networks 1 (1–2) (2005) 89–124.
[5] P. Medagliani, J. Leguay, V. Gay, M. Lopez-Ramos, G. Ferrari, Engineering energy-efficient target detection applications in wireless sensor networks, in: Proc. 8th IEEE Int. Conf. on Pervasive Computing and Communications, PerCom 2010, Mannheim, Germany, 2010, 9 pages.
[6] L. Lazos, R. Poovendran, J.A. Ritcey, Analytic evaluation of target detection in heterogeneous wireless sensor networks, Transactions on Sensor Networks 5 (2) (2009) 1–38.
[7] L.A. Santalò, M. Kac, Integral Geometry and Geometric Probability, Cambridge University Press, Cambridge, UK, 2004.
[8] H. Solomon, Geometric Probability, SIAM, Philadelphia, PA, 1978.
[9] N. Zhao, L. Sun, Research on cross-layer frameworks design in wireless sensor networks, in: Proc. of 3rd Int. Conf. on Wireless and Mobile Communications, ICWMC 07, Guadeloupe, France, 2007, p. 50a.
[10] T. Melodia, M.C. Vuran, D. Pompili, The state of the art in cross-layer design for wireless sensor networks, in: Proc. of EuroNGI Work. on Wireless and Mobility, Springer Lecture Notes on Computer Science, LNCS, vol. 388, Como, Italy, 2005.
[11] Q. Cao, T. Yan, J.A. Stankovic, T. Abdelzaher, Analysis of target detection performance for wireless sensor networks, in: Proc. of First IEEE Conf. on Distributed Computing in Sensor Systems, DCOSS 2005, Marina del Rey, CA, 2005, pp. 276–292.
[12] Y. Ting, Analysis approaches for predicting performance of wireless sensor networks, Ph.D. Thesis, Charlottesville, VA, advisor: Stankovic, J.A. (2006).
[13] Y. Zhu, Y. Liu, L. Ni, Z. Zhang, Low-power distributed event detection in wireless sensor networks, in: Proc. of the 26th IEEE Int. Conf. on Computer Communications, INFOCOM 07, Anchorage, AK, 2007, pp. 2401–2405.
[14] J. Zhang, M. Walpola, D. Roelant, H. Zhu, K. Yen, Self-organization of unattended wireless acoustic sensor networks for ground target tracking, Pervasive and Mobile Computing 5 (2) (2009) 148–164.
[15] Y. Cao, B. Yang, Intruding target detection using wireless sensor network, in: Proc. of 9th International Conference on Electronic Measurement Instruments, ICEMI 2009, Beijing, China, 2009, pp. 2–1015 –2–1020.
[16] Q. Wu, M. Zhu, N. Rao, Integration of sensing and computing in an intelligent decision support system for homeland security defense, Pervasive and Mobile Computing 5 (2) (2009) 182–200.
[17] T. He, S. Krishnamurthy, L. Luo, T. Yan, L. Gu, R. Stoleru, G. Zhou, Q. Cao, P. Vicaire, J.A. Stankovic, T.F. Abdelzaher, J. Hui, B. Krogh, Vigilnet: an integrated sensor network system for energy-efficient surveillance, Transactions on Sensor Networks 2 (1) (2006) 1–38.
[18] Crossbow Website, http://www.xbow.com.
[19] H. Zhang, J. Hou, Is deterministic deployment worse than random deployment for wireless sensor networks? in: Proc. of 25th IEEE Conference on Computer Communications, INFOCOM 06, Barcelona, Spain, 2006, 13 pages.
[20] J. Wang, S. Medidi, Energy efficient coverage with variable sensing radii in wireless sensor networks, New York City, NY, 2007, p. 61.
[21] M. Younis, K. Akkaya, Strategies and techniques for node placement in wireless sensor networks: a survey, Journal of Ad Hoc Networks 6 (4) (2008) 621–655.
[22] P. Medagliani, J. Leguay, G. Ferrari, V. Gay, M. Lopez-Ramos, Accurate performance bounds for target detection in WSNs with deterministic node placement, in: Proc. of IEEE Int. Symp. on Wireless Pervasive Computing, ISWPC 10, Modena, Italy, 2010, 6 pages.
[23] Z. Yuan, G. Wang, Sensor deployment strategy for collaborative target detection with guaranteed accuracy, Wuhan, China, 2008, pp. 68–71.
[24] R. Tan, G. Xing, J. Wang, H.C. So, Collaborative target detection in wireless sensor networks with reactive mobility, in: Proc. of the 16th Int. Work. on Quality of Service, IWQoS 2008, Enschede, Netherlands, 2008, pp. 150–159.
[25] Micaz datasheet http://www.xbow.com/Products/Product_pdf_files/wireless_pdf/micaz_datasheet.pdf.
[26] J. Polastre, R. Szewczyk, D. Culler, Telos: enabling ultra-low power wireless research, in: Proc. of the 4th Int. Symp. on Information Processing in Sensor Networks, IPSN 05, Piscataway, NJ, 2005, pp. 364–369.
[27] M. Buettner, G. Yee, E. Anderson, R. Han, X-mac: a short preamble mac protocol for duty-cycled wireless sensor networks, in: Proc. of 4th ACM Int. Conf. on Embedded networked sensor systems, SenSys 06, Boulder, CO, 2006, pp. 307–320.
[28] K. Klues, G. Hackmann, O. Chipara, C. Lu, A component-based architecture for power-efficient media access control in wireless sensor networks, in: Proc. of the 5th ACM Int. Conf. on Embedded networked sensor systems, SenSys 07, Sidney, Australia, 2007, pp. 59–72.
[29] A. Papoulis, Probability, Random Variables and Stochastic Processes, McGraw-Hill, New York, NY, 1991.
[30] J.R. Taylor, An Introduction to Error Analysis: The Study of Uncertainties in Physical Measurements, 2nd ed., University Science Books, 1996.
[31] J. Polastre, J. Hill, D. Culler, Versatile low power media access for wireless sensor networks, in: Proc. of 2nd ACM Int. Conf. on Embedded Networked Sensor Systems, SenSys 04, Baltimore, MD, 2004, pp. 95–107.
[32] O.K. Tonguz, G. Ferrari, Ad Hoc Wireless Networks: A Communication-Theoretic Perspective, 2006.
[33] D. Bertsekas, R. Gallager, Data Networks, 2nd ed., Prentice-Hall, Upper Saddle River, NJ, 1992.
[34] D. Bertsimas, J. Tsitsiklis, Introduction to Linear Optimization, Athena Scientific, Belmont, MA, 1997.
[35] Y. Gu, J. Hwang, T. He, D.H. Chang Du, Usense: a unified asymmetric sensing coverage architecture for wireless sensor networks, in: Proc. of the 27th Int. Conf. on Distributed Computing Systems, ICDCS 2007, Toronto, Ontario, Canada, 2007.